Optimum access waveguide width for $1 \times N$ multimode interference couplers on silicon nanomembrane

Amir Hosseini,[1,*] Harish Subbaraman,[2] David Kwong,[1] Yang Zhang,[1] and Ray T. Chen[1,3]

[1]*Microelectronic Research Center, Department of Electrical and Computer Engineering, University of Texas, 10100 Burnet Road, Austin, Texas 78758, USA*

[2]*Omega Optics, Inc., 10306 Sausalito Drive, Austin, Texas 78759, USA*

[3]*E-mail: raychen@uts.cc.utexas.edu*

**Corresponding author: ahoss@mail.utexas.edu*

Received June 10, 2010; accepted July 23, 2010;
posted August 5, 2010 (Doc. ID 129863); published August 19, 2010

We derived an analytical formula for the optimum width of the access waveguides of $1 \times N$ multimode interference (MMI) couplers. Eigenmode-decomposition-based simulations show that the optimum width relation corresponds to the points of diminishing returns in both insertion loss and output uniformity versus access waveguide width. We fabricate and characterize 1×12 MMI couplers on a nanomembrane of silicon-on-insulator substrate. The experimental investigations demonstrate that the analytical results can be reliably used as a design rule for MMI couplers with large number of outputs. © 2010 Optical Society of America

OCIS codes: 130.3120, 130.2790.

Multimode interference (MMI) devices based on self-imaging are key components in photonic integrated circuits (PICs). Many $1 \times N$ MMI-device-based beam splitters have been theoretically and experimentally investigated [1–6]. The resolution and contrast of the images formed in the multimode waveguide determine the uniformity and insertion loss of MMI splitter devices [1]. By analyzing the phase errors due to deviations of the higher-order-mode dispersion relations from those required for ideal self-imaging, one can show that MMI couplers with a large number of outputs (N) normally result in poorer output uniformity and higher insertion loss [2]. There have been two major techniques proposed to enhance MMI coupler performance: optimizing the index contrast [2,3] and increasing the input/output access waveguide width [4]. Other approaches, such as using a genetic algorithm [5] and tuning the input taper angle [6], were also investigated.

Tuning the index contrast may not be an option, based on the choice of the substrate and the geometry of the splitter. Also, use of genetic algorithm or input taper angle tuning does not provide insight into the nature of the poor MMI coupler performance at large N values. Increasing the input/output access waveguide width to enhance the self-imaging quality proposed in [4] is a practical approach, especially for cases such as PICs, where index tuning is a challenge. In this study, we investigate the effect of the input/output access waveguide width on the MMI coupler performance and derive an analytical relation for the optimum width for minimizing insertion loss and enhancing output uniformity. Experimental results for a 1×12 MMI device based on a silicon nanomembrane confirm the analytical conclusions.

The theory of self-imaging in multimode optical waveguides has been the subject of several studies [1,7–9]. Figure 1 shows a schematic of a $1 \times N$ MMI splitter. The multimode waveguide section consists of a W_{MMI} wide and L_{MMI} long core with refractive index n_c. In the case of channel waveguides, an equivalent 2D representation can be made by techniques such as the effective index method or the spectral index method [7].

Assume that n_{eff} is the effective index of the fundamental mode of an infinite slab waveguide with same thickness and claddings. For each mode $p (0 \le p \le M)$ of an MMI coupler that can support $(M+1)$ modes, the dispersion relation is given as [1]

$$\beta_p^2 + \kappa_{yp}^2 = \left(\frac{2\pi n_{\mathrm{eff}}}{\lambda_0}\right)^2, \tag{1}$$

where β_p is the propagation constant of the pth mode and λ_0 is the free-space wavelength. Throughout this Letter, $\lambda_0 = 1.55$ μm. k_{yp} is the lateral wavenumber of the pth mode given as $k_{yp} = (p+1)\pi/W_e$, where W_e is the effective width, which includes the penetration depth due to the Goose–Hahnchen shift [7]. In the MMI theory, β_p is approximated from Eq. (1) as [1]

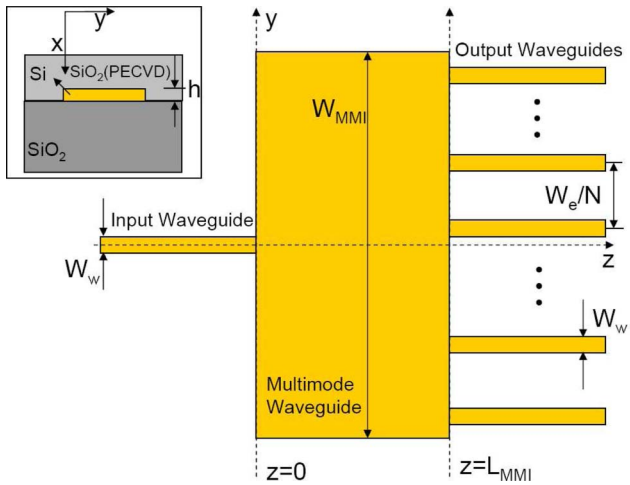

Fig. 1. (Color online) Schematic of a $1 \times N$ MMI beam splitter. Inset is a cross-sectional schematic of the SOI waveguiding structure. $n_{\mathrm{si}} = 3.47$, $n_{\mathrm{SiO_2}} = 1.45$, and $n_{\mathrm{SiO_2\,(PECVD)}} = 1.46$.

$$\beta_p \approx \beta_0 - \frac{p(p-2)}{3L_\pi}, \tag{2}$$

where $L_\pi/(\beta_o-\beta_1) \approx 4n_{\text{eff}}W_e^2/3\lambda_0$. In the case of symmetric excitations, such as a $1 \times N$ MMI coupler excited by the fundamental mode of the input waveguide, using the approximation in Eq. (2), one can show that the required length for such a coupler is $L_{\text{MMI}} = 3IL_\pi/4N$, where I is an integer. However, MMI couplers with their length derived using the approximation in Eq. (2) suffer from high insertion loss and poor output uniformity, as discussed in [2]. The approximation in Eq. (2) becomes increasingly inaccurate for larger-mode numbers (p), which results in larger accumulated modal phase errors in the multimode section at the output with regard to the values required for ideal self-imaging. It was shown before that increasing the input/output waveguide width (W_w) improves the image quality by reducing the accumulated modal phase errors at the output of the multimode section [4]. However, the maximum W_w is limited by the geometry as well as the coupling between the output waveguides. Also, larger W_w results in longer tapers when the output channels are adiabatically tapered down for single-mode operation. Our goal is to find the minimum W_w for which the MMI coupler performance is still acceptable.

The error in the calculated propagation constant when using Eq. (2) can be estimated by the third term in the Taylor expansion of β_p given by Eq. (1) as $\Delta\beta_p \approx 2(k_{yp}\lambda_0/4\pi n_{\text{eff}})^4$. After propagating along the MMI device, the resulting modal phase errors at the output are given as

$$\Delta\varphi_p = \Delta\beta_p L_{\text{MMI}} = \frac{\pi\lambda_0^2(p+1)^4}{64N{n_{\text{eff}}}^2W_e^2}. \tag{3}$$

For a high-quality image at the output of the MMI device, we restrict the maximum $\Delta\varphi_p$ to $\pi/2$, because if $\Delta\varphi_p$ is more than $\pi/2$, the sign of the mode field p is changed by the phase error. Let q be the maximum mode number (p) for which $\Delta\varphi_p < \pi 2$. We choose W_w so that the highest-order mode excited in the multimode region can satisfy this restriction. To do so, we pick W_w to be equal to the lateral wavelength ($2\pi/k_{yq}$) of the highest allowed mode given by $\Delta\varphi_p < \pi 2$. This also guarantees negligible excitation of all higher order modes, because several periods of these modes fall within the input excitation field and the resulting overlap integrals are, thus, small. By equating $W_{w,\text{opt}} = 2\pi/k_{yq}$, we get

$$W_{w,\text{opt}} = \frac{1}{\sqrt[4]{2N}}\sqrt{\frac{\lambda_0 W_e}{n_{\text{eff}}}}. \tag{4}$$

When $W_w \geq W_{w,\text{opt}}$, the $\Delta\varphi_p < \pi/2$ condition holds for all the modes in the multimode section that receive significant excitation. Therefore, we expect that $W_{w,\text{opt}}$ corresponds to the point of diminishing returns (or the knee point) in $1 \times N$ MMI coupler performance in terms of insertion loss and output uniformity as functions of W_w.

To investigate the effect of W_w on image quality, we used the 3D full vectorial eigenmode expansion simulator in the FIMMPROP module from Photon Design. We calculated MMI device outputs from the transfer matrix coefficients of the fundamental mode in the output channels. We assumed silicon nanomembrane on oxide, as shown in the Fig. 1 inset, where the thickness of the silicon slab is $h = 230$ nm ($n_{\text{eff}} = 2.85$).

For given W_{MMI} and W_w, one can tune L_{MMI} to achieve better uniformity [5]. To demonstrate that tuning the MMI device length to achieve high-output uniformity and high transmission is an inefficient method, let us consider a 1×12 MMI coupler with $W_{\text{MMI}} = 60$ μm. For this MMI coupler, the theoretical predictions give $L_{\text{MMI}} = 553.4$ μm and $W_{w,\text{opt}} = 2.58$ μm. Figures 2(a) and 2(b) show the insertion loss and output uniformity, respectively, for varying L_{MMI} and for $W_w = 0.5$ μm, $W_w = 1.25$ μm, $W_w = 2.6$ μm, and $W_w = 3.5$ μm. Uniformity is calculated as $10\ \log(P_{\text{min}}/P_{\text{max}})$, where P_{max} and P_{min} are the maximum and minimum power (norm of the fundamental mode) of the MMI device output channels, respectively.

In the case of $W_w = 1.25$ μm and $W_w = 0.5$ μm, the highest uniformity does not occur at the lowest insertion loss and the resulting optimized MMI coupler length is different from the theoretical predictions, as shown in Fig. 2. For $W_w = 2.6$ μm and $W_w = 3.5$ μm, the optimum lengths are closer to $L_{\text{MMI}} = 553.4$ μm, at which the total insertion loss is also much smaller than that for $W_w = 1.25$ μm and $W_w = 0.5$ μm. Also, the MMI device performance is almost the same for $W_w = 2.6$ μm and $W_w = 3.5$ μm.

To verify the $W_{w,\text{opt}}$ values predicted by Eq. (4), we simulated MMI couplers with different N values. Figures 2(c) and 2(d) show the insertion loss and the

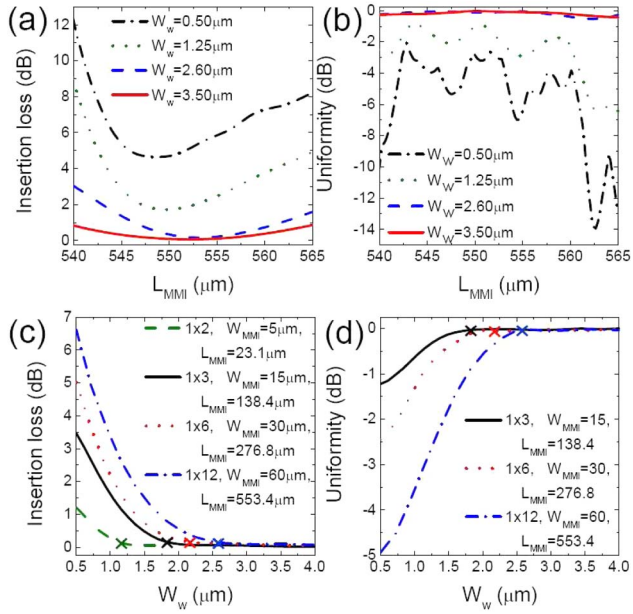

Fig. 2. (Color online) (a), (b) Variations of the insertion loss and output uniformity, respectively, versus MMI coupler length. The MMI device is 1×12 ($N = 12$), $W_{\text{MMI}} = 60$ μm, $h = 230$ nm, and different W_w values. (c), (d) Variations of the insertion loss and output uniformity, respectively, versus W_w for 1×12, 1×3, 1×6, and 1×12 MMI couplers. Because of symmetry, uniformity is 0 dB for all W_w values in the case of the 1×2 MMI coupler. $W_{w,\text{opt}}$ values for each MMI device are indicated by crosses (×).

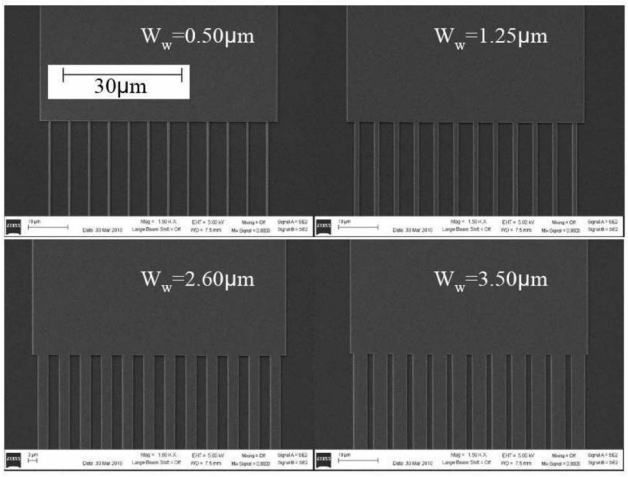

Fig. 3. (a) Scanning electron microscope pictures of 1×12 MMI couplers with $W_{\mathrm{MMI}}60$ μm, $L_{\mathrm{MMI}} = 553.4$ μm, and different W_w.

output uniformity, respectively, versus the W_w for 1×2, 1×3, 1×6, and 1×12 MMI couplers. The MMI device dimensions are shown in the figure, and the MMI device lengths are $3L_\pi/4N$ in all cases. Using Eq. (4), the corresponding $W_{w,\mathrm{opt}}$ values are 1.16 μm, 1.82 μm, 2.17 μm, and 2.58 μm for the 1×2, 1×3, 1×6, and 1×12 MMI couplers, respectively. One can see that these numbers correspond to the points of diminishing returns in both the total output power and uniformity versus W_w. Also note that when the access waveguide width (W_w) is less than the $W_{w,\mathrm{opt}}$ value, larger MMI couplers have worse permanence than smaller MMI couplers. Thus, it is more crucial to apply $W_w \geq W_{w,\mathrm{opt}}$ as a design rule for larger MMIs.

We fabricated 1×12 MMI couplers ($W_{\mathrm{MMI}} = 60$ μm, $W_{\mathrm{MMI}} = 553.4$ μm) with $W_w = 0.50$ μm, $W_w = 1.25$ μm, $W_w = 2.60$ μm, and $W_w = 3.50$ μm [see Fig. 3]. The MMI couplers are fabricated on a silicon-on-insulator (SOI) substrate with a 3 μm buried oxide layer. The MMI devices are patterned using electron-beam lithography, followed by reactive ion etching, lift-off pattern inversion, and plasma-enhanced chemical vapor deposition (PECVD) of a 1-μm-thick silicon dioxide film for the top cladding. The details of the fabrication process will be reported separately. The output waveguides are fanned out for 30 μm center-to-center separation.

A TE field from an external-cavity tunable laser source is coupled into the input waveguides through a tapered and lensed polarization-maintaining fiber. A CCD camera captured top-down images of the scattered light at the cleaved output waveguide facets, as shown in Figs. 4(a) and 4(b). For the same input power, we observed significantly brighter outputs for the $W_w = 2.60$ μm and $W_w = 3.50$ μm MMI couplers compared to the $W_w = 0.50$ μm and $W_w = 1.25$ μm MMI couplers.

To calculate the output uniformity, a single-mode output fiber is scanned at the output side across each output waveguide cross section for maximum output coupling. In order to cancel out the fabrication errors, we use the average of output fiber measurement results from two sets of the four MMI devices. Figures 4(c) and 4(d) compare the measured insertion loss and output uniformity values with those from the simulation results shown in Figs. 2(c) and 2(d). The results from both simulation and experimental data indicate that $W_w = 2.60$ μm, which is predicted from Eq. (4), is, in fact, the point of diminishing returns for the MMI coupler performance as a function of the width of the access waveguides.

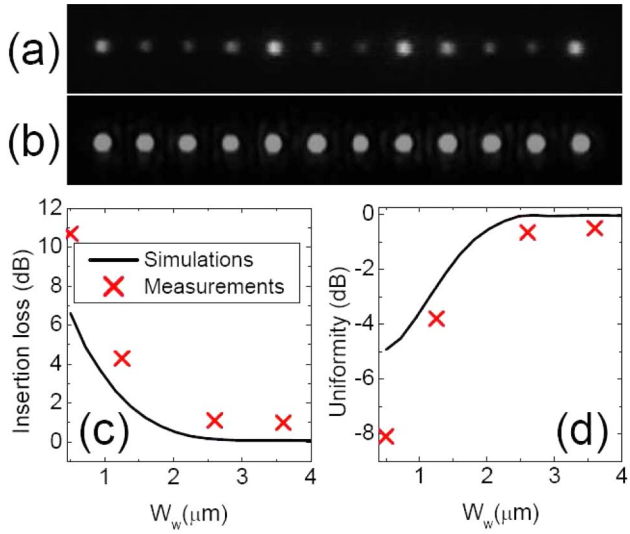

Fig. 4. (Color online) Top-down IR images of MMI device outputs for (a) $W_w = 0.50$ μm, and (b) $W_w = 2.60$ μm. (c) and (d) Insertion loss and uniformity measurement results for 1×12 MMI couplers with $W_{\mathrm{MMI}} = 60$ μm, $L_{\mathrm{MMI}} = 553.4$ μm, and different W_w values, respectively.

An analytical formula for optimum $1 \times N$ multimode input/output access waveguide width is derived for improved performance based on the insertion loss and the output uniformity. Eigenmode-decomposition-based simulations and experimental investigations of SOI-based 1×12 MMI couplers confirm the analytical results. The results can be used as a design rule for high-performance MMI-coupler-based beam splitters.

This research is supported by the Multidisciplinary University Research Initiative (MURI) program through the United States Air Force Office of Scientific Research (USAFOSR), contract FA 9550-08-1-0394.

References

1. R. Ulrich and T. Kamiya, J. Opt. Soc. Am. **68**, 583 (1978).
2. J. Z. Huang, R. Scarmozzino, and R. M. Osgood, Jr., IEEE Photon. Technol. Lett. **10**, 1292 (1998).
3. R. Yin, J. Yang, X. Jiang, J. Li, and M. Wang, Opt. Commun. **181**, 317 (2000).
4. Y. Shi, D. Dai, and S. He, Opt. Commun. **253**, 276 (2005).
5. Q. Wang, J. Lu, and S. He, Opt. Commun. **209**, 131 (2002).
6. R. M. Lorenzo, C. Llorenle, E. J. Abril, and M. López, Proc. Inst. Elect. Eng. Optoelectron. **145**, 65 (1998).
7. L. Soldano and E. Pennings, J. Lightwave Technol. **13**, 615 (1995).
8. M. Rajarajan, B. Rahman, T. Wongcharoen, and K. Grattan, J. Lightwave Technol. **14**, 2078 (1996).
9. A. Hosseini, D. N. Kwong, C.-Y. Lin, B. S. Lee, and R. T. Chen, IEEE J. Sel. Top. Quantum Electron. **6**, 53 (2010).